Ecological Complexity 20 (2014) 185–194

Contents lists available at ScienceDirect

Ecological Complexity

journal homepage: www.elsevier.com/locate/ecocom

Original Research Article

Plankton blooms and patchiness generated by heterogeneous physical environments

Michael Bengfort [a,*], Ulrike Feudel [b], Frank M. Hilker [a], Horst Malchow [a]

[a] Institute of Environmental Systems Research, School of Mathematics/Computer Science, Osnabrück University, Barbarastr. 12, 49069 Osnabrück, Germany
[b] Institute for Chemistry and Biology of the Marine Environment, Theoretical Physics/Complex Systems, Carl von Ossietzky University Oldenburg, Carl von Ossietzky Str. 9–11, 26111 Oldenburg, Germany

ARTICLE INFO

Article history:
Received 1 August 2014
Received in revised form 30 September 2014
Accepted 11 October 2014
Available online

Keywords:
Plankton
Predator–prey systems
Two dimensional flows
Reaction-diffusion equations
Eddy diffusion

ABSTRACT

Microscopic turbulent motions of water have been shown to influence the dynamics of microscopic species living in that habitat. The number, stability, and excitability of stationary states in a predator–prey model of plankton species can therefore change when the strength of turbulent motions varies. In a spatial system these microscopic turbulent motions are naturally of different strength and form a heterogeneous physical environment. Spatially neighboring plankton communities with different physical conditions can impact each other due to diffusive coupling. We show that local variations in the physical conditions can influence the global system in form of propagating pulses of high population densities. For this we consider three different local predator–prey models with different local responses to variations in the physical environment. The degree of spatial heterogeneity can, depending on the model, promote or reduce the number of propagating pulses, which can be interpreted as patchy plankton distributions and recurrent blooms.

1. Introduction

Organisms in the ocean crucially depend on their physical environment. Therefore, biological–physical interactions have a great impact on the spatial distribution, growth, and dominance of species. Of particular interest are flow patterns in the ocean which influence marine organisms on all spatial scales (Mann and Lazier, 1996). Large-scale flow patterns across the equatorial Pacific which are related to the El Niño phenomenon considerably diminish the plankton and subsequently the fish production at the South American coast (Marzeion et al., 2005; Heinemann et al., 2011). Mesoscale hydrodynamic flow patterns like jets and vortices are responsible for the emergence of filamental plankton patterns (Tél et al., 2005; Hernández-García et al., 2002; Sandulescu et al., 2007) which in turn have a large impact on growth, coexistence, and dominance of species (Hernández-García and López, 2004; Neufeld and Hernández-Garcia, 2010; Scheuring et al., 2003; Bastine and Feudel, 2010). Abraham (1998), McKiver and Neufeld (2011), Hernández-García et al. (2002) and Tzella and Haynes (2007) used a carrying capacity which can be transported by the flow, but has a fixed spatial distribution of its source, to explain the generation of plankton patchiness. Since the seminal paper by Abraham (1998), the influence of stirring and mixing in the ocean on plankton patchiness and blooms has become an important topic of current research.

In addition to the already mentioned large and mesoscale hydrodynamic flows, small-scale turbulence contributes to the redistribution of nutrients as well as the behavior of plankton, and has therefore been considered in various models.

There are many studies, showing that turbulence can affect the behavior and health of plankton species themselves. Visser and Stips (2002) and Kiørboe and Saiz (1995) analyzed the effect of microscopic turbulence on encounter rates, feeding currents, signal detection, behavior, and prey selection of copepods. Visser et al. (2009) studied the optimal behavior of zooplankton in a turbulent environment. MacKenzie and Leggett (1991) quantified the contribution of small-scale turbulence to the encounter rates between larval fish and their zooplankton prey. Metcalfe et al. (2004) modeled a plankton foodweb in environments with different turbulent levels and therefore different values of nutrient uptake rates (half-saturation coefficients) and predator–prey capture rates. Peters and Marrasé (2000) gave an overview of some experimental data from different laboratory

* Corresponding author. Tel.: +49 5419692573; fax: +49 5419692599.
E-mail address: mbengfort@uni-osnabrueck.de (M. Bengfort).

http://dx.doi.org/10.1016/j.ecocom.2014.10.003
1476-945X/

studies and made some theoretical considerations. Peters et al. (2006) studied the effects of small-scale turbulence on the growth of two diatoms of different size in a phosphorus-limited medium. However, these studies have investigated the effect of turbulence on plankton species or communities from a "local" point of view. They have not taken into account systems of species which live in regions of different strength of turbulence and may be spatially connected.

Our aim is therefore to develop a model which couples plankton population dynamics to hydrodynamic motion, including the effect of the heterogeneous environment on biological growth. We further investigate if these effects can be a mechanism for plankton patchiness or plankton blooms.

In the following section, we point out some possible effects of turbulent environments on plankton systems and develop different models which take into account these impacts. We begin with "local" models consisting of ordinary differential equations that ignore spatial fluxes. Nevertheless, we show that the effects of turbulence included in those models can influence the number and stability of stationary states of the system.

We then extend the models by incorporating spatial dynamics. Our simulations show that a spatially inhomogeneous distribution of turbulence strength has varied impacts on the whole excitable system and is able to trigger or to suppress propagating pulses of high population concentrations, corresponding to plankton blooms and patchiness.

2. General biological model

Since our main focus is on plankton dynamics in aquatic environments, we consider phytoplankton P and zooplankton Z as the major components of the biological system.

We focus on excitable predator–prey models based on the model introduced by Truscott and Brindley (1994) to explain the emergence of large plankton blooms such as red tides:

$$\begin{cases} \dfrac{dZ}{dt} &= \dfrac{aP^n}{h^n+P^n}Z - m_Z Z^q, \\ \xi\dfrac{dP}{dt} &= rP\left(1-\dfrac{P}{K}\right) - \dfrac{aP^n}{h^n+P^n}Z, \end{cases} \tag{1}$$

where P denotes the phytoplankton density as the prey and Z is the zooplankton density corresponding to the predators. In the absence of predators, P grows logistically with the maximum per capita growth rate r until it reaches the carrying capacity K. P is grazed upon by Z with the maximal grazing rate a. h is the half-saturation density of prey, so that the factor $(P^n)/(h^n + P^n) = 0.5$ for $P = h$. The type of functional response is defined by n. If $n = 1$, the predator grazes with a Holling-type II functional response. If $n = 2$, grazing is of Holling-type III. q gives the order of the predator mortality (Edwards and Yool, 2000). We analyze models with a linear predator mortality ($q = 1$) and a model with quadratic mortality ($q = 2$). A quadratic predator mortality is motivated by possible intraspecific competition or the existence of a top predator, which is not explicitly modeled. m_Z is the predator's per capita mortality rate. ξ is a factor describing the different timescales of the dynamics of the two different species (Sieber et al., 2007).

All quantities are non-dimensional in this paper (see Appendix A).

The predator–prey models have a trivial stationary state $(P^{(1)}, Z^{(1)}) = (0, 0)$, a semi-trivial stationary state $(P^{(2)}, Z^{(2)}) = (K, 0)$, and, depending on the set of parameters, one or more non-trivial stationary states in the positive quadrant of the phase-plane.

2.1. Possible effects of turbulent flows on the vital parameters and feeding behavior

In this section we point out how turbulent motion on the length scale of the diameter of plankton cells can influence the parameters of the system (1).

Experimental results show that in a low turbulent regime only insignificant effects on plankton organism can be observed (Peters and Marrasé, 2000). In an intermediate turbulent environment, positive effects on growth rates of phytoplankton and capture rates of zooplankton were measured; in highly turbulent environments insignificant or negative effects were found. However, negative effects were observed for unrealistically strong turbulence, which cannot be observed in oceans but only in cultures with artificial turbulence.

According to our aim to investigate the influence of small-scale turbulence on plankton growth, we consider two possible mechanisms of how turbulence can change the growth rates of phyto- and zooplankton. On the one hand, we assume that a higher turbulence level increases the zooplankton capture rate of phytoplankton. On the other hand, we incorporate a turbulence-dependent growth of phytoplankton in our model. For the latter, we suppose that turbulent mixing leads to a homogenization of the nutrient distribution reflected by a turbulence-dependent carrying capacity.

Regarding turbulence-dependent zooplankton growth, we base our model on some experimental results. Peters et al. (2006) observed more *Coscinodiscus* sp. (a species of diatoms) cells in a turbulent environment than under still water conditions with low nutrient concentrations. They explained this observation by comparing these experimental results to a model using the Michaelis–Menten nutrient uptake model with a turbulence-dependent half-saturation constant. Metcalfe et al. (2004) used the same ansatz and provided values for the half-saturation constant for copepods and ciliates between 71 nmol P l^{-1} in a non-turbulent environment and 44 nmol P l^{-1} in a turbulent environment with a high turbulent kinetic energy dissipation.

To study the impact of turbulence on the growth of zooplankton we adopt the ideas of Peters et al. (2006) and introduce a turbulence-dependent half-saturation constant $h \equiv h(turb)$ in the predator functional response. For an example, we illustrate this for the Holling-type III functional response g_{H3}:

$$g_{H3}(P, turb) := \frac{aP^2}{h^2(turb) + P^2}, \tag{2}$$

where P is the density of prey, and a the maximal ingestion rate of the predator. The normalized parameter $turb$, with $0 \le turb \le 1$, describes the relative strength of turbulence.

We define

$$h(turb) = \frac{h_0}{1 + turb \cdot c_h} \tag{3}$$

as the turbulence-dependent half-saturation density, where h_0 is the maximal half-saturation density. The explicit dependence of h on $turb$ can be influenced by the parameter c_h. We use this simple dependence on turbulence, but in a more complex model c_h can be a function of $turb$ as well.

Regarding the turbulence-dependent phytoplankton growth in an environment with high nutrient concentration, we use a logistic model for the growth of phytoplankton. In a static environment, the cell depletes the nutrients in its near surrounding. New nutrients can enter this zone by molecular diffusion from the nutrient rich environment. If the population of the phytoplankton cells is very high, it might be that other cells deplete the near surrounding as well. Light can be diminished because of self-shading. In a turbulent environment clusters of cells will be segregated, the nutrient

depleted-zone around a single cell becomes permanently renewed, and each cell have access to the same mean light intensity.

We can model this as a negative effect of still environments on the logistically growing species:

$$\frac{dP}{dt} = rP\left(1 - \frac{P}{K(turb)}\right) \tag{4}$$

The turbulence-dependent carrying capacity $K(turb)$ is defined as follows:

$$K(turb) = K_0 + turb \cdot c_K, \tag{5}$$

where K_0 describes the minimal carrying-capacity of the prey. Similar to the turbulence-dependent half-saturation density (Eq. (3)), the dependence of the carrying capacity can be varied by c_K.

The influence of turbulence cannot only be described by varying the parameters of the equations describing the biological dynamics. Some species are forced to change their behavior in a turbulent environment, which also can be included in our model. If a predator is hunting in an area with low prey density, it may migrate into another area if it is not successful in finding food for some time (Anderson et al., 2012). This behavior can be modeled by a sigmoid functional response (Luck et al., 1979; Real, 1977). A turbulent environment would disturb the predator, making it harder or even unnecessary to behave like this because the turbulent medium force the plankton to some random motion. Morozov (2010) showed that the sigmoid grazing function (Holling-type III) is realistic for heterogeneous prey distributions while in a well mixed homogeneous environment the predators' behavior has to be described less sigmoid (Holling-type I or II). Therefore we model the change in the predators behavior by changing from a Holling-type III functional response in a non-turbulent environment, to Holling-type II in a strongly turbulent, and therefore well mixed, environment.

For this, we use the following functional response $g(P, turb)$:

$$g(P, turb) := turb \cdot \frac{aP}{h(turb) + P} + (1 - turb) \cdot \frac{aP^2}{h(turb)^2 + P^2}, \tag{6}$$

which is a convex combination of the type II and III functional responses. Note that for $turb = 1$, we get the type II functional response, and for $turb = 0$, we get the type III functional response. For $0 < turb < 1$, we get a functional response in between.

In the following section we take a look at different models of the form (1). The first one will show the effect of turbulence-dependent parameters K and h in a system with Holling-type III functional response ($n = 2$), whereas the predator mortality is thought to be linear ($q = 1$). In the second model we additionally assume that the predator changes its behavior as described in Eq. (6), and model III will be a variant of model I with a quadratic predator mortality ($q = 2$).

3. Specific predator–prey models

In this section we look at three specific predator–prey models. For all models we use the following set of parameters which are adopted from Sieber et al. (2007):

$$r = 1, \quad a = 1/9, \quad m_Z = 0.0525, \quad \xi = \frac{1}{10}. \tag{7}$$

Moreover, we choose the following values of h_0 and c_h, to ensure that at least one locally stable stationary state in our models is stable.

$$h_0 = 1/16, \quad c_h = 0.4, \quad K_0 = 0.7, \quad c_K = 0.3. \tag{8}$$

For $turb = 1$ we get $K(turb) = 1$, which is identical to the carrying capacity used by Sieber et al. (2007). However, the parameters r, a, m_Z, $K(1)$ and $h(1)$ are, in their dimensional version, similar to the parameters used by Truscott and Brindley (1994).

A general feature of the models we discuss in the following is that they all have an excitable stationary state for these parameter values. Excitability means that certain small but over-critical perturbations from the stable stationary state can result in a huge response of the system, namely the formation of a large phytoplankton concentration, before the system returns to the stable stationary state.

3.1. Predator–prey model I: linear predator mortality

First we concentrate on the effect of turbulence on the parameters K and h:

$$\frac{dZ}{dt} = [g_{H3}(P, turb) - m_Z] \cdot Z, \tag{9}$$

$$\xi\frac{dP}{dt} = \left[r\left(1 - \frac{P}{K(turb)}\right) - \frac{aP}{h^2(turb) + P^2}Z\right] \cdot P. \tag{10}$$

The predator density is constant if Eq. (9) becomes zero. This is the case for $Z = 0$ and for a particular prey concentration

$$P_0(turb) = \sqrt{\frac{m_Z h^2(turb)}{a - m_Z}}. \tag{11}$$

The prey density stops varying in time if $P = 0$ or if Z fulfills the equation of the non-trivial nullcline

$$Z_0(P, turb) = \frac{r\left(1 - \frac{P}{K(turb)}\right)}{aP}\left(h^2(turb) + P^2\right). \tag{12}$$

This model possesses one stationary state where predator and prey can coexist. This non-trivial stationary state $(P^{(3)}, Z^{(3)})$ where the two nullclines intersect is the only stable stationary state of this model using the parameter-set (7) and (8).

$$(P^{(3)}, Z^{(3)}) = (P_0(turb), Z_0(P_0(turb), turb)). \tag{13}$$

$(P^{(3)}, Z^{(3)})$ is stable if the determinant of the Jacobian matrix is positive and the trace is negative. The first condition leads to $h(turb) < K(turb)\sqrt{a - m_Z/m_Z}$ if $m_z < a$ and the second condition gives $h(turb) > (1 - a/2m_Z)K(turb)\sqrt{a - m_z/m_Z}$ for $a > m_Z$. With the chosen parameters (7) and (8) both conditions are always true.

When increasing turbulence, the non-trivial stationary state moves along the nullcline $Z_0(P, turb)$ to smaller prey densities (Fig. 1). The system is excitable as long as the predator nullcline P_0

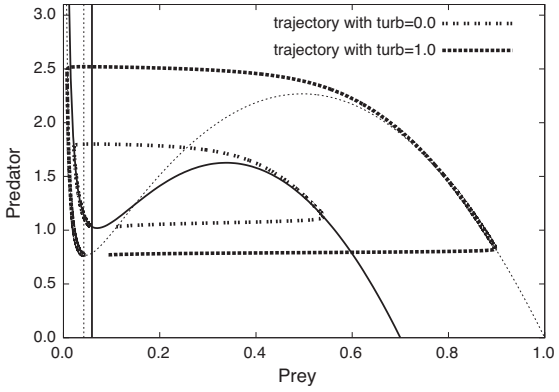

Fig. 1. Nullclines of model I. Dashed lines: $turb = 1$; solid lines: $turb = 0$; additionally, a trajectory for each value of $turb$ is plotted which starts at a position near the stationary state shifted to higher values of P ($P(t = 0) = P^{(3)} + \Delta P$ with $\Delta P = 0.05$). The trajectories then grow to higher values of P and Z before they end at the stationary state. With increased $turb$ the system reaches higher density values during the excitation.

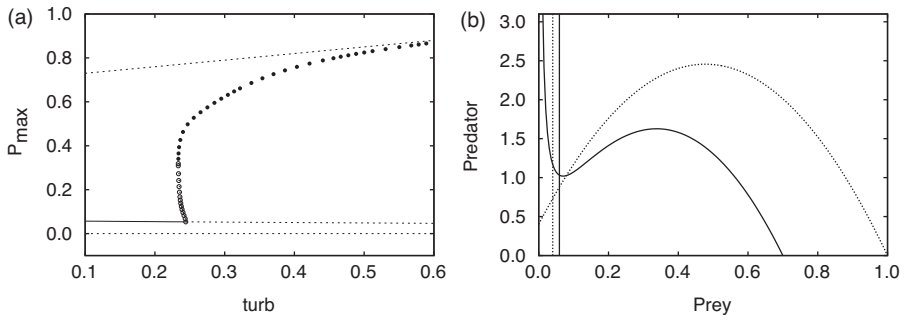

Fig. 2. (a) Bifurcation diagram. Dashed lines: unstable stationary states, solid line: stable stationary state, empty circles: maximal prey-density of unstable limit cycles, filled circles: maximal prey density of stable limit cycles. (b) Nullclines of model II. Dashed lines $turb = 1$; solid lines $turb = 0$.

intersects the prey nullcline Z_0 at the left of the local minimum of Z_0. After the phytoplankton concentration reaches the nullcline $Z_0(P, turb)$ during an excitation, the zooplankton population increases as well and the system returns to the stationary state. To illustrate this, one trajectory for the system with $turb = 0$ and one for the system with $turb = 1$ is added to Fig. 1. Both trajectories start close to the stationary state and return after a long journey though phase space, passing high prey and predator densities. The maximum of these excitations depends on the carrying capacity K and, therefore, on the parameter *turb*.

3.2. Predator–prey model II: changing grazing behavior

In our second model we consider the case where the predator can switch its feeding behavior according to the turbulence level (see Eq. (6)):

$$\begin{cases} \dfrac{dZ}{dt} &= g(P, turb)Z - m_Z Z, \\ \xi \dfrac{dP}{dt} &= rP\left(1 - \dfrac{P}{K(turb)}\right) - g(P, turb)Z. \end{cases} \tag{14}$$

In numerical simulations with low values of *turb*, this system behaves similarly to the one discussed before. However, at a certain level of turbulence, the stationary state loses stability in a subcritical Hopf bifurcation (Fig. 2a). For a very small range of the parameter *turb* there is a stable and an unstable periodic solution which coexist with the stable non-trivial stationary state. For larger values of *turb* only the stable periodic solution remains. The system then behaves periodically without any excitations. The reason for this is that the prey nullcline (Fig. 2b)

$$Z_0(P, turb) = r\left(1 - \frac{P}{K(turb)}\right) \frac{1}{(1 - turb)\frac{aP}{h(turb)^2 + P^2} + turb\frac{a}{h(turb)+P}} \tag{15}$$

changes from a function with two local extrema in the positive quadrant to a function with one single extremum in the positive quadrant when increasing *turb*. For large values of *turb*, the stationary state $(P^{(3)}, Z^{(3)})$ loses stability and there is no stable stationary state in the positive quadrant any more. This is caused by the change of predator behavior as described in Eq. (6).

For large values of *turb*, the trajectory comes very close to the vertical axis $P = 0$ which is the stable manifold of the trivial solution (0, 0). Mathematically, P is always greater than zero. However, if we define a minimal viable population size $P_{\min}$ and set $P = 0$ for $P < P_{\min}$, both species go extinct.

3.3. Predator–prey model III: quadratic predator mortality

Now, model I is modified by introducing a quadratic mortality term in the predator dynamics:

$$\frac{dZ}{dt} = g_{H3}(P, turb)Z - m_Z Z^2, \tag{16}$$

$$\xi \frac{dP}{dt} = rP\left(1 - \frac{P}{K(turb)}\right) - g_{H3}(P, turb)Z. \tag{17}$$

This modification gives rise to a saddle-node bifurcation (Fig. 3a) yielding two additional stationary states, $(P^{(4)}, Z^{(4)})$ and $(P^{(5)}, Z^{(5)})$. $(P^{(4)}, Z^{(4)})$ is an unstable state while $(P^{(5)}, Z^{(5)})$ is locally stable. The system becomes bistable. Depending on the initial conditions the system converges to either one or the other stable stationary states. Note that the system can switch between the two locally stable stationary states if a perturbation of some kind pushes it into the basin of attraction of the other stationary state (Fig. 3b).

4. Spatial model

So far we have treated the impact of turbulence as an additional parameter, which is constant in space and time, and influences the

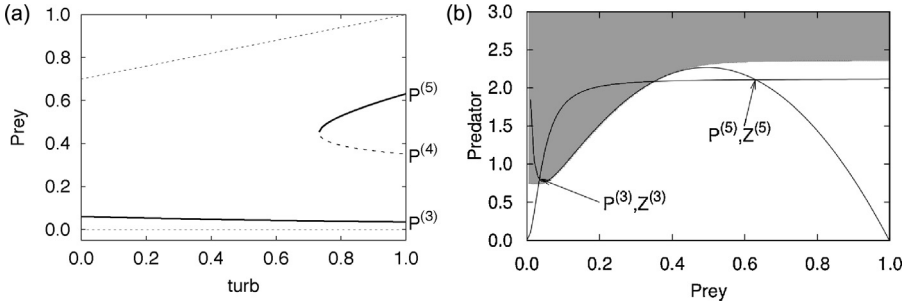

Fig. 3. (a) Bifurcation diagram. Solid lines represent stable, and dashed lines unstable stationary states. (b) Basin of attraction for $turb = 1.0$. Initial conditions inside the white area leading the system to the stationary state $(P^{(5)}, Z^{(5)})$, whereas the dark area leads to the stationary state $(P^{(3)}, Z^{(3)})$. Additionally, the nullclines of the system are shown.

behavior of the grazers and the growth parameters of the populations. In a real fluid, the turbulence level changes in space depending on the velocity field. However, to simplify our approach, we do not consider real turbulent fields. Instead we assume a velocity field which possesses certain features of an ocean flow. Using these features, we construct a spatially inhomogeneous distribution of the parameter *turb* to mimic spatially heterogeneous physical conditions. Therefore, we now consider the interplay of biological growth with inhomogeneous physical features in a spatial domain.

A typical feature in an ocean flow field is a rotating eddy. Lee (2012) showed that eddies may have some influence on predator–prey systems. In contrast to that work, we do not focus on species of a length scale similar to the eddy (e.g. fish), but on plankton species whose length scale is much smaller than the grid that we use to describe the eddy itself. We describe an eddy by the following stream function:

$$\Phi(\mathbf{x},t) = AR^2 \exp\left(-\frac{|\mathbf{x}-\mathbf{x}_0|^2}{2R^2}\right); \quad u = -\frac{\partial\Phi}{\partial y}; \quad v = \frac{\partial\Phi}{\partial x}. \tag{18}$$

$\mathbf{x} = (x, y)$ is a two-dimensional vector giving the position on the spatial grid, u is the resulting velocity in the horizontal direction (x) while v gives the velocity in the vertical direction (y). R is the radius of the eddy, $\mathbf{x}_0$ is the position of its center, and A is a factor to vary its strength. The resulting flow field is radially symmetric around the center $\mathbf{x}_0$ of the eddy (Fig. 4). Because everything would move in circles around $\mathbf{x}_0$, it is not necessary to look at the effect of advection in this flow.

A two-dimensional hydrodynamic flow can be characterized with the help of the strain tensors

$$S_n = \frac{\partial u}{\partial x} - \frac{\partial v}{\partial y} \quad \text{normal strain}, \tag{19}$$

$$S_s = \frac{\partial v}{\partial x} + \frac{\partial u}{\partial y} \quad \text{shear strain}. \tag{20}$$

Assuming that macroscopic strain leads to microscopic turbulence, we use the strength of the strain created by the flow as a quantity for turbulence:

$$\begin{aligned} turb &= norm(S_n^2 + S_s^2) \\ &= norm\left(\exp\left(-\frac{|\mathbf{x}-\mathbf{x}_0|^2}{2R^2}\right) \cdot \frac{|\mathbf{x}-\mathbf{x}_0|^2}{R^2} \cdot A\right)^2. \end{aligned} \tag{21}$$

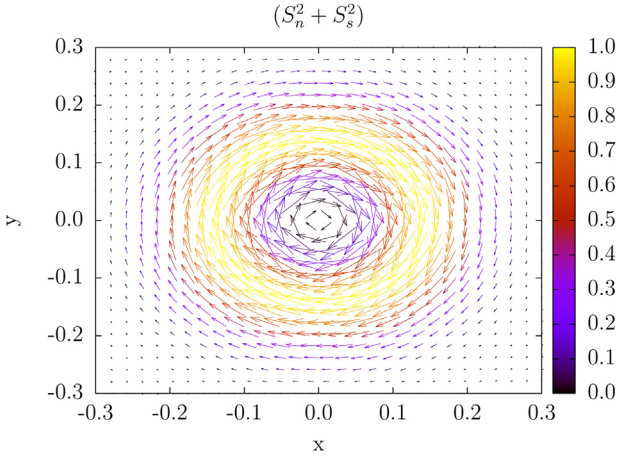

Fig. 4. Absolute strain rates $(S_n^2 + S_s^2)$ generated by a flow field of a single eddy. The velocity field is indicated by arrows. $R = 0.1$, $A = \exp(1)/2$, $x_0 = (0, 0)$.

norm is a factor to normalize *turb* so that $0 \le turb \le 1$. We set $A = \exp(1)/2$. In this case the maximal value of the squared absolute strain rate $S_n^2 + S_s^2$ is equal to 1 and therefore $norm = 1$.

This assumption is motivated by the stress-similarity model by Liu et al. (1994). The idea of this model is that velocities at different scales give rise to turbulent stress with similar structures. The subgrid-scaled turbulent motion can then be implemented as an increased coefficient of diffusion:

$$D = D_{\min} + turb \cdot (D_{\max} - D_{\min}). \tag{22}$$

$D_{\min}$ and $D_{\max}$ are the maximal and the minimal coefficients of diffusivity in the system. In our simulations we do not choose the values of D_{min} and D_{max} on the basis of experimental data, but we analyze the effect of different choices.

Now, we consider the following reaction-diffusion equations on a two dimensional grid with an inhomogeneously distributed diffusion coefficient which correlates with the parameter *turb*:

$$\begin{aligned} \frac{\partial Z}{\partial t} &= F_Z(P,Z) + \nabla(D(\mathbf{x})\nabla Z) \\ &= F_Z(P,Z) + (\nabla D(\mathbf{x}))(\nabla Z) + D(\mathbf{x})\nabla^2 Z, \end{aligned} \tag{23}$$

$$\begin{aligned} \frac{\partial P}{\partial t} &= \frac{1}{\xi} F_P(P,Z) + \nabla(D(\mathbf{x})\nabla P) \\ &= F_P(P,Z) + (\nabla D(\mathbf{x}))(\nabla P) + D(\mathbf{x})\nabla^2 P. \end{aligned} \tag{24}$$

$F_Z(P, Z)$ and $F_P(P, Z)$ are the equations of the biological reaction from Sections 3.1 to 3.3. For model I, for instance, this means $F_P(P, Z) = rP(1 - P/K) - (aP^2/(h^2 + P^2))Z$ and $F_Z(P, Z) = (aP^2/(h^2 + P^2))Z - m_Z Z$.

$\nabla = (\partial/\partial x, \partial/\partial y)$ is the two-dimensional Nabla operator. In case of a spatially constant coefficient of diffusion D, the factors $(\nabla D(\mathbf{x}))(\nabla Z)$ and $(\nabla D(\mathbf{x}))(\nabla P)$ vanish. We call these terms "*gradient terms*".

At the boundaries of the two-dimensional grid we use Neumann boundary conditions $\nabla Z = \nabla P = 0$.

The idea of spatially inhomogeneous diffusion coupled with inhomogeneous biological parameters has also been pursued by Shigesada et al. (1986, 1987). They studied the propagation of periodic waves on a grid with a periodical change in the coefficient of diffusion and the growth rate of the population. Lutscher et al. (2006), Mckenzie et al. (2012) and Jin et al. (2014) used a similar mechanism to explain the survival of species in a stream.

5. Numerical results

Because of the radial symmetry in our spatial model, we can restrict our attention to the one-dimensional problem along the radius of the eddy. Therefore we use the radial distance from the center of the eddy, r, as spatial parameter. As initial conditions we use the locally stable stationary state $(P^{(3)}, Z^{(3)})$ at all values of r for each model. If $(P^{(3)}, Z^{(3)})$ does not exist (model II at high values of *turb*), we use the last existing $(P^{(3)}, Z^{(3)})$ at lower values of *turb* instead.

5.1. Model I – spatially extended

Fig. 5 shows the value of *turb* as a function of the radial distance from the center of the eddy. Additionally Fig. 5 shows the stable states of model I when ignoring diffusion in Eqs. (23) and (24). These are the solutions of (9) and (10) which depend on the spatial location as *turb* varies with r. In the more turbulent regions around the eddy center the prey and predator densities are smaller than in the less turbulent regions.

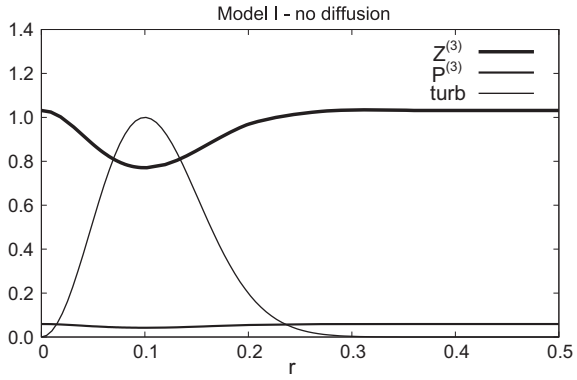

Fig. 5. Stable non-trivial states of model I without diffusion in a radial distance r from the eddy center $r = 0$. The higher the value of *turb*, the smaller the values of the stable stationary states $P^{(3)}$ and $Z^{(3)}$.

If the difference in population size between two spatial sites is large enough, diffusive coupling between the two locations may result in a perturbation that triggers a local excitation as shown in Fig. 1. Hence, when considering diffusion in Eqs. (23) and (24), the "local" system at a site may become excited and then "infect" the neighboring sites. Due to the radial symmetry of our flow field, this leads to a ring of excitation around the eddy which propagates through the entire excitable spatial system (see Fig. 6). After an excitation, the system returns to its initial state, and the ring of excitation starts again due to the trigger of diffusive fluxes.

The lower panels of Fig. 6 show the distribution of the parameter *turb* in space. The upper panels show the temporal and spatial changes of the plankton densities. Note that the densities in the area with high values of *turb* reach larger values during the excitation than in the less turbulent regions. By contrast, in the absence of diffusion, population sizes of both phyto- and zooplankton are smaller in the turbulent region (cf. Fig. 6). Hence, the rings of excitation lead to repeated spatiotemporal "blooms".

Depending on the parameters used in the model, the diffusive coupling has to exceed a certain critical value to excite the system. Two coupled local systems can only trigger an excitation if one local system is located in a particular area of the phase plane in relation to the other local system. This is illustrated in Fig. 7. If the coefficient of diffusion cannot link two local systems in such a way that they excite each other, no propagating pulses occur in the spatial system. Otherwise, propagating pulses occur and their frequency remains constant in this model.

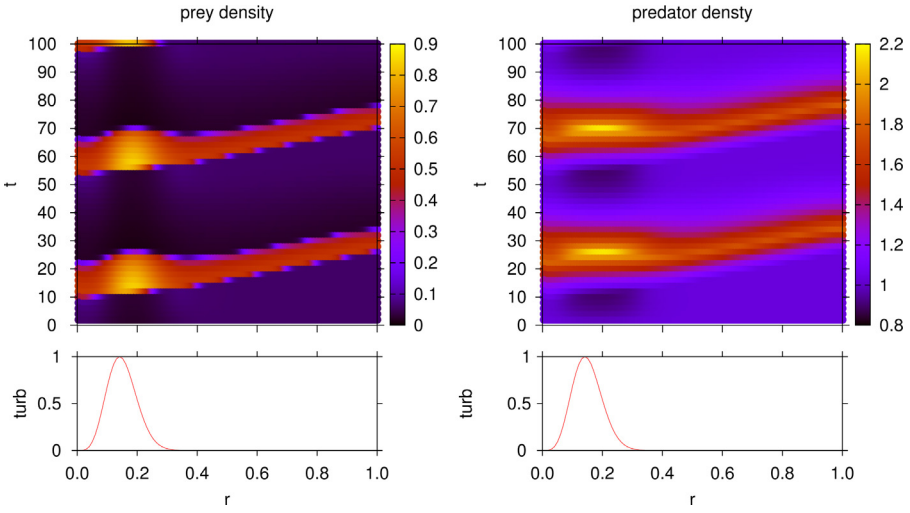

Fig. 6. Repeated excitations in model I with diffusion that form pulses in space and time for both prey and predator densities (upper panels). The lower panels show the turbulence profile that leads to local perturbations of population size triggering the excitations. Parameter values: $D_{min} = 5 \cdot 10^{-4}$, $D_{max} = 2.3 \cdot 10^{-3}$.

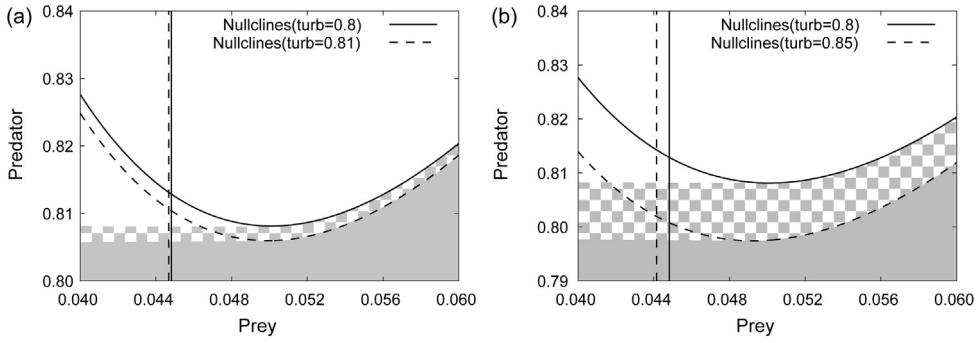

Fig. 7. Nullclines of model I. If the system is forced into the marked area below the nullclines, the system becomes excited. In panel (a) the dashed nullclines belong to a system with *turb* = 0.81. If the diffusive coupling can link this system with the system with *turb* = 0.8 (solid nullclines), no excitation occurs, because both stationary states are located in the non-excitable part of the phase plane (white area). In panel (b) the dashed nullclines belong to a system with *turb* = 0.85. The stationary state of this system is located in the area of the phase plane where the system with *turb* = 0.8 (solid and checked) becomes excited. A diffusive connection which is strong enough to link these two systems results in an excitation.

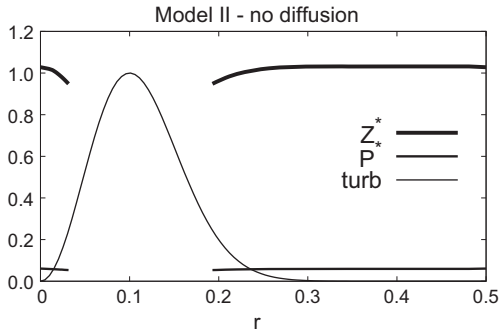

Fig. 8. Stable non-trivial states (P^* and Z^*) of model II without diffusion in a radial distance r from the eddy center $r = 0$. Around the maximal value of *turb* the system ends up in periodic solutions, which are not shown here.

5.2. Model II – spatially extended

Model II differs from model I by the fact that the area with high turbulence has no stable non-trivial state, but periodic solutions (Fig. 8). These periodic solutions can have high amplitudes (cf. Fig. 2a). At the beginning of the oscillation period the major change takes place in the prey density, whereas the predator density starts increasing with a certain time delay because of $\xi < 1$. So spatial sites which accommodate biological systems in the oscillatory state easily excite the neighboring sites even at very small coefficients of diffusion.

The resulting propagating pulses are similar to those in model I (Fig. 6), but occur even at very low values of the diffusivity.

5.3. Model III – spatially extended

For large values of *turb*, model III is bistable as there is an additional stable stationary state ($P^{(5)}$, $Z^{(5)}$) with large plankton densities. This is illustrated in Fig. 9 a for the spatially extended model III without diffusion.

When considering diffusion, we again use the stationary state at small plankton-densities ($P^{(3)}$, $Z^{(3)}$) as initial conditions. So before the first excitation occurs, model III with diffusion behaves similarly as model I with diffusion. However, if an excitation occurs, the plankton densities may reach such large values that they get attracted by the alternative stable state ($P^{(5)}$, $Z^{(5)}$) if this state exists, i.e. in the more turbulent area. Hence, after the first excitation, the system gets "caught" in the high-densities state in some spatial locations and does not return to the initial state with small plankton densities anymore. Therefore, it is already clear that model III can behave profoundly differently in space and time than model I.

Once the populations are "caught" in ($P^{(5)}$, $Z^{(5)}$) in the turbulent area, we can observe two different scenarios. First, the diffusive coupling between states with large ($P^{(5)}$, $Z^{(5)}$) and small ($P^{(3)}$, $Z^{(3)}$) densities can result in an excitation of the excitable system. In this case, a pulse of excitation starts from the interface between ($P^{(5)}$, $Z^{(5)}$) and ($P^{(3)}$, $Z^{(3)}$), i.e. the eddy boundaries. This is illustrated in Fig. 9b, where a pulse of excitation propagates radially away from the eddy. Secondly, if the differences in population size between ($P^{(5)}$, $Z^{(5)}$) and ($P^{(3)}$, $Z^{(3)}$) and the gradient of the diffusivity profile are too large, the gradient terms $(\nabla D)(\nabla P)$ and $(\nabla D)(\nabla Z)$ become large and important. They represent an extra positive term for both phytoplankton and zooplankton in Eqs. (23) and (24), respectively, at the eddy boundary and in its center. While an increase in phytoplankton density tends to promote excitability, an increase in zooplankton tends to reduce excitability (cf. the phase plane portrait in Fig. 3a). Simulations performed indicate that the latter effect seems to prevail. This is illustrated in Fig. 9c, where a

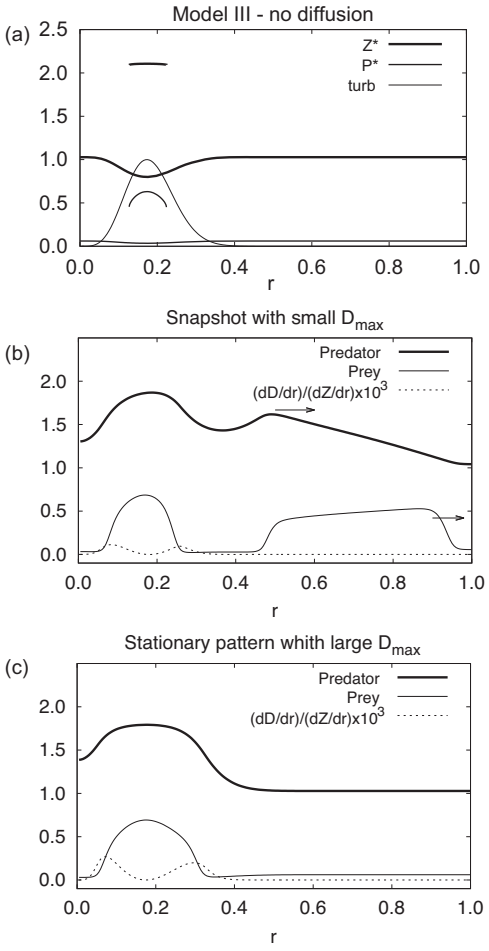

Fig. 9. Dynamics of model III. (a) Stable non-trivial stationary states (P^* and Z^*) with no diffusion. The area around the maximal *turb* is bistable. (b) Snapshot at $t = 77$ for small $D_{max} = 9.5 \cdot 10^{-4}$. The arrows indicate the direction of the propagating pulses which start from the eddy. (c) Stationary pattern for large $D_{max} = 2.3 \cdot 10^{-3}$. No propagating pulses occur for large *gradient terms*. In the area of high *turb* the system remains in a state of high densities. The dashed line shows the *gradient term* for the predator dynamics $(\nabla D)(\nabla Z)$ multiplied with the factor 1000. In panels (b) and (c) the minimal coefficient of diffusion is $D_{min} = 5 \cdot 10^{-4}$.

large difference in diffusivities prevent excitations. In the turbulent area, the system remains in the alternative stable state with large densities. This is a stationary pattern that does not change in time, in particular, there are no propagating pulses of excitation.

5.4. Frequency of propagating pulses

To summarize this section we point out that there is one effect which occurs in all three spatial models: If the timescale factor is much less than 1 ($\xi \ll 1$), the eddy creates rings of excitation in the surrounding system. Those excitations propagate through the system radially away from the eddy center (see Fig. 6 as an example.) This result is similar to Muratov et al. (2007) who generated propagating pulses of excitation with additive noise in excitable systems.

The velocity of the radial pulses generated in excitable media has been computed by Keener (1980). For $\xi \ll 1$ it mainly depends on ξ^{-1}. Differences in the frequency in which they are generated depend on the model and the spatial distribution of D. Fig. 10 shows the number of propagating pulses running through the system (we count the number of times the densities exceed a certain value and go back to lower values again at the right boundary of the system.).

We can observe the following effects in the three models considered. In the case of a spatially constant coefficient of

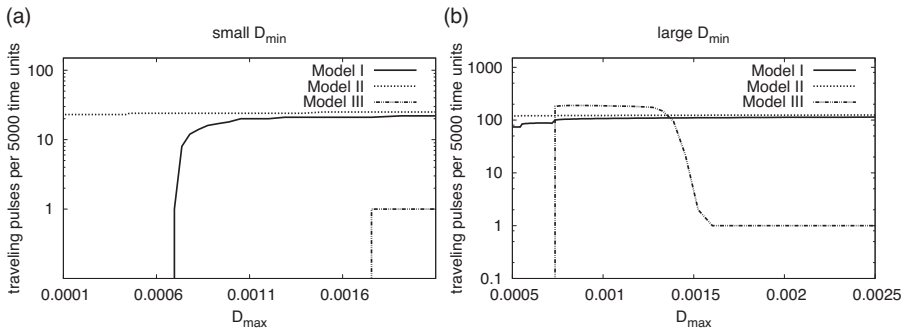

Fig. 10. Number of propagating pulses in the first 5000 time units. The same position on the horizontal axis of each panel gives the same value of $\Delta D(r) = D_{max} - D_{min}$. (a) $D_{min} = 1 \cdot 10^{-4}$: with increasing D_{max} the strength of the diffusivity $D(r)$ also increases at the edge of the turbulent area and propagating pulses occur in model II. In model III only one propagating pulse has been counted at high D_{max}. Model I shows propagating pulses at all values of D_{max}. (b) $D_{min} = 5 \cdot 10^{-4}$: there is a range of values D_{max} which allow many propagating pulses in model III. Model I exhibits pulses of excitations for all values of D_{max}, as diffusivity is generally large enough.

diffusion we have $D_{max} = D_{min}$ and have to consider the smallest values shown on the horizontal axes in Fig. 10 (which are intersected by the vertical axes). For model I, the diffusivity in panel a is not strong enough to trigger pulses of excitation. For a higher diffusivity (panel b) excitations are observed in model I, even without a diffusion gradient. Model II shows propagating pulses of excitation in both cases of low and high diffusivity, because the oscillations in the local model provide large enough perturbations to trigger excitations independently of the diffusivity (as long as $D(r) > 0$ for all r). Model III is similar to model I after starting the simulation with the initial conditions; both panels do not show any excitations for this model when diffusivities are spatially constant. This is caused by the fact that the stationary state $(P^{(3)}, Z^{(3)})$ in the local model III is not exactly identical with the one in model I. So there is a higher coefficient of diffusion needed to start excitations in model III than in model I.

In the case of spatially heterogeneous coefficients of diffusion $D(r)$, i.e. $D_{max} > D_{min}$, the pulse frequency varies with the maximum coefficient of diffusion D_{max}, with the minimum coefficient of diffusion D_{min} being held constant in each panel of Fig. 10. In general, increasing D_{max} also increases $\nabla D = (D_{max} - D_{min}) \nabla\, turb$ and thus renders the gradient terms non-negligible.

If the minimal coefficient of diffusion does not allow excitations in model I (Fig. 10a), propagating pulses occur in the system beyond a certain maximal coefficient of diffusion D_{max}. At this value of D_{max}, the local diffusivity at the edges of the high turbulent area is large enough to make an excitation possible. If the minimal diffusion coefficient is large enough (Fig. 10b), propagating pulses occur for all values of D_{max}.

Model II shows no significant changes in the case of heterogeneous coefficients of diffusion, because the oscillations in the local model in the turbulent regions allow excitations even at small coefficients of diffusion.

For model III, a sufficiently large value of D_{max} leads to exactly one pulse of excitation. This is because after the first excitation, the system remains in the stable state $(P^{(5)}, Z^{(5)})$ with high *turb*, and the *gradient terms* prevent further excitations. This effect holds for both low and high diffusivities (Fig. 10a and b, respectively). However, if diffusivity is high (Fig. 10b), there is a range of values of D_{max} where repeated pulses of excitation take place. Here the diffusivity is strong enough to make excitation possible from the initial conditions, but the gradient ∇D is small enough not to suppress further propagating pulses.

6. Discussion and conclusion

The aim of our investigation is to examine how heterogeneous environmental conditions can influence a predator–prey system. These heterogeneities are based on a different strength of turbulent motion in the environment. We have found that these heterogeneities can produce pulses of high plankton densities, which propagate through the global spatial system.

We considered three different predator–prey models with implementations of turbulence-dependent parameters. All models are based on the Truscott–Brindley model. The first model used a Holling-type III functional response with turbulence-dependent half-saturation density, logistic prey growth with turbulence-dependent carrying capacity and linear predator mortality. The second model added the scenario that the predator changes its behavior by switching from a functional response of type II to type III with increasing turbulence. Model III used a quadratic predator mortality.

We used a single set of parameters for the three models. Other dynamics than those shown in this paper are possible if other parameter values are used. Nevertheless we have shown that turbulence can influence the number and stability of stationary states of the local models described by ordinary differential equations. Even though the effect of turbulence on each species in the phenomenological descriptions (i.e. Eqs. (3) and (5)) is positive, the stationary state in the interaction of both species can be at lower population densities, so that the total effect of turbulence on the phytoplankton biomass is negative. Hence, the influence of turbulence on the plankton ecosystem cannot be completely understood by looking at a single species alone. Instead we have to take a look at the interaction of different species in such systems as well.

In space, the excitable models behave differently in different areas of a heterogeneous environment. Diffusive coupling of neighboring areas leads to global effects. Local turbulence not only changes the plankton concentrations locally, but also has the ability to produce pulses of high plankton densities which propagate through the whole system. This was shown with a simple one-dimensional reaction-diffusion model and can be one candidate mechanism creating plankton blooms and patchiness.

It turns out that excitability in the spatial systems is dependent on the timescale factor ξ and the gradient of the eddy diffusion $\nabla D(\mathbf{r})$. For weaker eddies ($A < exp(1)/2$), the parameter *turb* does not reach the value 1. This also influences the excitability of the spatial system. The way the parameters *turb*, D_{max} and D_{min} are linked is important for the dynamics of the entire system. *turb* represents the local microscopic turbulence on the length scale of plankton as a parameter for the ordinary differential equations, D_{min} and D_{max} are simple descriptions of these turbulent motions on the macroscopic level.

While space-dependent parameters of the biological model generate propagating pulses through the excitable spatial system, the space-dependent diffusivity may support (model I) or suppress (model III) the propagation of these pulses, or has no influence

(model II). In the first case, the support is a result of the locally increased diffusion. In the second case, the suppression is a result of the higher plankton concentration at high values of *turb* and the resulting positive effect of the *gradient terms*. If there are strong local variations in the plankton dynamics like in model II, the spatial dependence of the coefficient of diffusion has no significant effect.

Interestingly, previous work on population dynamics in streams and rivers has shown that rotational flow, caused by obstacles (e.g., stones) interrupting the constant water flow in a stream, can positively affect prey and predator survival (Lee, 2012). Similarly, Scheuring et al. (2003) argued that the strong chaotic mixing of a viscous water flow around an obstacle can promote the coexistence of competing species. In both cases, the flow creates small-scale mosaics that shift in space and time, and benefit the populations. In this paper, we show that the spatial inhomogeneity induced by a rotating eddy can augment or diminish local population size and, more importantly, can create global phenomena like repeated propagating pulses.

Modeling turbulence by linking macroscopic strain rates to turbulent diffusion (Section 4) is a simplification. Yet, with the help of this model, we managed to easily relate pattern formation on a macroscopic spatial level to the local behavior the ordinary differential equations. In this model we are able to compute a heterogeneous spatial environment from a static analytical flow field and use the strain rates as a source for the local microscopic turbulent motion which influences the plankton dynamics. This seems to be useful and comprehensible in the context of our qualitative investigations, but cannot be used to simulate realistic hydrodynamical problems. In future work, we plan to implement a biological model into a more realistic three-dimensional advection–diffusion model and compare the result to our two dimensional approximations.

Moreover, we simplify the influence of turbulence on plankton in the way that we assume the same mechanism and dependencies on an average of plankton organisms of different size and species (Granata and Dickey, 1991; Karp-Boss et al., 1996; Kiørboe and Saiz, 1995; MacKenzie and Leggett, 1991). Future work could investigate the competition of species with different responses to turbulent environments.

In reality, turbulence varies not only in space, but also in time. The combination of spatially and temporally varying parameters could lead to further interesting effects. For instance, it has been shown that the interplay of spatial inhomogeneities and temporal variability can lead to emergent phenomena such as an invasion ratchet, describing seasonal invasion dynamics (Jin et al., 2014).

Another interesting investigation would be to analyze the influence of turbulence on the infection rate of diseases (Kühn and Hofmann, 1999; Llaveria et al., 2010) and the resulting spatial distribution of infected organisms.

Appendix A. A dimensionless predator–prey model

We want to obtain a dimensionless version of the dimensional system

$$\frac{\mathrm{d}Z}{\mathrm{d}t} = \frac{\alpha a P^n}{h^n + P^n} Z - m_Z Z^q = F_Z(P, Z), \tag{25}$$

$$\xi \frac{\mathrm{d}P}{\mathrm{d}t} = rP\left(1 - \frac{P}{K}\right) - \frac{aP^n}{h^n + P^n} Z = \xi F_P(P, Z). \tag{26}$$

Therefore we set $z = Z/(\alpha P_0)$, $p = P/P_0$, $\tau = t/t_0$ and get

$$\frac{\mathrm{d}z}{\mathrm{d}\tau} = \frac{a' p^n}{h'^n + p^n} z - m'_Z z^q = f_p(p, z), \tag{27}$$

$$\xi \frac{\mathrm{d}p}{\mathrm{d}\tau} = r' p\left(1 - \frac{p}{K'}\right) - \frac{a' p^n}{h'^n + p^n} z = f_z(p, z) \tag{28}$$

with $a' = a\alpha t_0$, $h' = h/P_0$, $m'_Z = m_Z t_0 (P_0\alpha)^{q-1}$, $r' = rt_0$ and $K' = K/P_0$. P_0 is a constant parameter with the dimension of a density while t_0 is a constant parameter with dimension time.

In the same way we can write a dimensionless version of the reaction-diffusion equations:

$$\frac{\partial X_i}{\partial t} = F_i(P, Z) + (\nabla D)(\nabla X_i) + D\nabla^2 X_i; \quad X_i \in \{P, Z\}. \tag{29}$$

With $d = Dx_0^2/t_0$, where the constant x_0 is a characteristic length scale, we get:

$$\frac{\partial x_i}{\partial \tau} = f_i(p, z) + (\nabla d)(\nabla x_i) + d\nabla^2 x_i; \quad x_i \in \{p, z\}. \tag{30}$$

$f_i(p, z)$ with $i \in \{P, Z\}$ are dimensionless versions of the system equations $F_Z(P, Z)$ and $F_P(P, Z)$.

References

Abraham, E.R., 1998. The generation of plankton patchiness by turbulent stirring. Nature 391, 577–580.

Anderson, K.E., Hilker, F.M., Nisbet, R.M., 2012. Directional biases and resource-dependence in dispersal generate spatial patterning in a consumer–producer model. Ecol. Lett. 15 (3), 209–217.

Bastine, D., Feudel, U., 2010. Inhomogeneous dominance patterns of competing phytoplankton groups in the wake of an island. Nonlinear Process. Geophys. 17 (6), 715–731.

Edwards, A.M., Yool, A., 2000. The role of higher predation in plankton population models. J. Plankton Res. 33, 1085–1112.

Granata, T., Dickey, T., 1991. The fluid mechanics of copepod feeding in a turbulent flow: a theoretical approach. Progr. Oceanogr. 26 (3), 243–261.

Heinemann, M., Timmermann, A., Feudel, U., 2011. Interactions between marine biota and ENSO: a conceptual model analysis. Nonlinear Process. Geophys. 18, 29–40.

Hernández-García, E., López, C., 2004. Sustained plankton blooms under open chaotic flows. Ecol. Complex. 1, 253.

Hernández-García, E., López, C., Neufeld, Z., 2002. Small-scale structure of non-linearly interacting species advected by chaotic flows. Chaos: Interdiscip. J. Nonlinear Sci. 12 (2), 470–480.

Jin, Y., Hilker, F.M., Steffler, P.M., Lewis, M.A., 2014. Seasonal invasion dynamics in a spatially heterogeneous river with fluctuating flows. Bull. Math. Biol. 76 (7), 1522–1565.

Karp-Boss, L., Boss, E., Jumars, P.A., 1996. Nutrient fluxes to planktonic osmotrophs in the presence of fluid motion. Oceanogr. Mar. Biol. 34, 71–107.

Keener, J., 1980. Waves in excitable media. SIAM J. Appl. Math. 39, 528–548.

Kiørboe, T., Saiz, E., 1995. Planktivorous feeding in calm and turbulent environments, with emphasis on copepods. Mar. Ecol. Progr. Ser. 122, 135–145.

Kühn, S.F., Hofmann, M., 1999. Infection of *Coscinodiscus granii* by the parasitoid nanoflagellate *Pirsonia diadema*: III. Effects of turbulence on the incidence of infection. J. Plankton Res. 21 (12), 2323–2340.

Lee, S.-H., 2012. Effects of uniform rotational flow on predator–prey system. Physica A: Stat. Mech. Appl. 391 (23), 6008–6015.

Liu, S., Meneveau, C., Katz, J., 1994. On the properties of similarity subgrid-scale models as deduced from measurements in a turbulent jet. J. Fluid Mech. 275, 83–119.

Llaveria, G., Garcés, E., Ross, O.N., Figueroa, R.I., Sampedro, N., Berdalet, E., 2010. Small-scale turbulence can reduce parasite infectivity to dinoflagellates. Mar. Ecol. Progr. Ser. 412, 45–56.

Luck, Robert, F., van Lenteren, J.C., Twine, P.H., Kuenen, L., Unruh, T., 1979. Prey or host searching behavior that leads to a sigmoid functional response in invertebrate predators and parasitoids. Res. Popul. Ecol. 20, 257–264.

Lutscher, F., Lewis, M., McCauley, E., 2006. Effects of heterogeneity on spread and persistence in rivers. Bull. Math. Biol. 68 (8), 2129–2160.

MacKenzie, E., Leggett, W., 1991. Quantifying the contribution of small-scale turbulence to the encounter rates between larval fish and their zooplankton prey: effects of wind and tide. Mar. Ecol. Progr. Ser. 73, 149–160.

Mann, K., Lazier, J., 1996. Dynamics of Marine Ecosystems. Blackwell Publishing, Oxford.

Marzeion, B., Timmermann, A., Murtugudde, R., Jin, F.-F., 2005. Biophysical feedbacks in the tropical pacific. J. Clim. 18, 58–70.

Mckenzie, H., Jin, Y., Jacobsen, J., Lewis, M.A., 2012. r_0 analysis of a spatiotemporal model for a stream population. SIAM J. Appl. Dyn. Syst. 11, 567–596.

McKiver, W.J., Neufeld, Z., 2011. Resonant plankton patchiness induced by large-scale turbulent flow. Phys. Rev. E 83 (January), 016303.

Metcalfe, A.M., Pedley, T., Thingstad, T., 2004. Incorporating turbulence into a plankton foodweb model. J. Mar. Syst. 49, 105–122.

Morozov, A.Y., 2010. Emergence of Holling-type III zooplankton functional response: bringing together field evidence and mathematical modelling. J. Theor. Biol. 265, 45–54.
Muratov, C.B., Vanden-Eijnden, E., Weinan, E., 2007. Noise can play an organizing role for the recurrent dynamics in exitable media. Proc. Natl. Acad. Sci. U. S. A. 104, 702–707.
Neufeld, Z., Hernández-Garcia, E., 2010. Chemical and Biological Processes in Fluid Flows. Imperial College Press, London.
Peters, F., Arin, L., Marrasé, C., Berdalet, E., Sala, M., 2006. Effects of small-scale turbulence on the growth of two diatoms of different size in a phosphorus-limited medium. J. Mar. Syst. 61, 134–148.
Peters, F., Marrasé, C., 2000. Effects of turbulence on plankton: an overview of experimental evidence and some theoretical considerations. Mar. Ecol. – Progr. Ser. 205, 291–306.
Real, L.A., 1977. The kinetics of functional response. Am. Nat. 111 (978), 289–300.
Sandulescu, M., López, C., Hernández-García, E., Feudel, U., 2007. Plankton blooms in vortices: the role of biological and hydrodynamic time scales. Nonlinear Process. Geophys. 14 (February), 443–454.
Scheuring, I., Károlyi, G., Toroczkai, Z., Tél, T., Péntek, A., 2003. Competing populations in flows with chaotic mixing. Theor. Popul. Biol. 63, 77–90.
Shigesada, N., Kawasaki, K., Teramoto, E., 1986. Traveling periodic waves in heterogeneous environments. Theor. Popul. Biol. 30, 143–160.
Shigesada, N., Kawasaki, K., Teramoto, E., 1987. The speeds of traveling frontal waves in heterogeneous environments. In: Teramoto, E., Yamaguti, M. (Eds.), Mathematical Topics in Population Biology, Morphogenesis and Neurosciences. Vol. 71 of Lecture Notes in Biomathematics. Springer, Berlin/Heidelberg, pp. 88–97.
Sieber, M., Malchow, H., Schimansky-Geier, L., 2007. Constructive effects of environmental noise in an excitable prey–predator plankton system with infected prey. Ecol. Complex. 4, 223–233.
Tél, T., de Moura, A., Grebogi, C., Károlyi, G., 2005. Chemical and biological activity in open flows: a dynamical system approach. Phys. Rep. 413 (2–3), 91–196.
Truscott, J., Brindley, J., 1994. Ocean plankton populations as excitable media. Bull. Math. Biol. 56 (5), 981–998.
Tzella, A., Haynes, P.H., 2007. Small-scale spatial structure in plankton distributions. Biogeosciences 4 (2), 173–179.
Visser, A.W., Mariani, P., Pigolotti, S., 2009. Swimming in turbulence: zooplankton fitness in terms of foraging efficiency and predation risk. J. Plankton Res. 31 (2), 121–133.
Visser, A.W., Stips, A., 2002. Turbulence and zooplankton production: insights from PROVESS. J. Sea Res. 47 (3–4), 317–329.